ARL-TR-8192 ● Oct 2017

US Army Research Laboratory

Process Development for Reactive-Ion Etching of Molybdenum (MoS_2) Utilizing a Poly(methyl methacrylate) (PMMA) Etch Mask

by Alin Cristian Chipara, Alexander L Mazzoni, Robert A Burke, Barbara M Nichols, Matthew L Chin, Sina Najmaei, Eugene Zakar, and Madan Dubey

NOTICES

Disclaimers

The findings in this report are not to be construed as an official Department of the Army position unless so designated by other authorized documents.

Citation of manufacturer's or trade names does not constitute an official endorsement or approval of the use thereof.

Destroy this report when it is no longer needed. Do not return it to the originator.

ARL-TR-8192 ● OCT 2017

US Army Research Laboratory

Process Development for Reactive-Ion Etching of Molybdenum (MoS_2) Utilizing a Poly(methyl methacrylate) (PMMA) Etch Mask

by Alin C Chipara and Alexander L Mazzoni
Oak Ridge Associated Universities (ORAU) Maryland, Belcamp, MD

Robert A Burke
General Technical Services, LLC, Wall Township, NJ

Barbara M Nichols, Matthew L Chin, Sina Najmaei, Eugene Zakar, and Madan Dubey
Sensors and Electron Devices Directorate, ARL

REPORT DOCUMENTATION PAGE

Form Approved
OMB No. 0704-0188

1. REPORT DATE *(DD-MM-YYYY)*	2. REPORT TYPE	3. DATES COVERED (From - To)
October 2017	Technical Report	January 2017–June 2017

4. TITLE AND SUBTITLE

Process Development for Reactive-Ion Etching of Molybdenum Disulfide (MoS_2) Utilizing a Poly(methyl methacrylate) **(**PMMA) Etch Mask

5a. CONTRACT NUMBER

5b. GRANT NUMBER

5c. PROGRAM ELEMENT NUMBER

6. AUTHOR(S)

Alin Cristian Chipara,* Alexander L Mazzoni,* Robert A Burke, Barbara M Nichols, Matthew L Chin, Sina Najmaei, Eugene Zakar, and Madan Dubey

5d. PROJECT NUMBER

5e. TASK NUMBER

5f. WORK UNIT NUMBER

7. PERFORMING ORGANIZATION NAME(S) AND ADDRESS(ES)

US Army Research Laboratory
ATTN: RDRL-SER-L
Adelphi, MD 20783-1138

8. PERFORMING ORGANIZATION REPORT NUMBER

ARL-TR-8192

9. SPONSORING/MONITORING AGENCY NAME(S) AND ADDRESS(ES)

10. SPONSOR/MONITOR'S ACRONYM(S)

11. SPONSOR/MONITOR'S REPORT NUMBER(S)

12. DISTRIBUTION/AVAILABILITY STATEMENT

Approved for public release; distribution is unlimited.

13. SUPPLEMENTARY NOTES

*These two authors contributed equally as co-first authors of this report.

14. ABSTRACT

Previously we have relied on a carbon tetraflouride (CF_4) + oxygen (O_2) reactive-ion etching recipe (15 sccm CF_4, 5 sccm O_2, and 200 W) to etch molybdenum disulfide (MoS_2). To define locations to be etched, the common electron beam lithography resist poly(methyl methacrylate) (PMMA) is used. However, we have observed that this process can leave a significant amount of PMMA residue on the substrate surface if the PMMA removal process is not aggressive enough. Additionally, this $CF_4 + O_2$ process etches silicon dioxide, which is typically used as both the substrate and back-gate dielectric of our 2-D field effect transistors. The PMMA residue tends to form a flap at the edge of the etched region instead of the PMMA particulate matter commonly reported in the 2-D literature. This report details the experiments performed to determine the source of the PMMA residue and the reasoning for switching to a chlorine + O_2 process with a secondary, pure O_2 step. This process development should be of use to others fabricating devices with 2-D materials or those using PMMA during reactive-ion etching.

15. SUBJECT TERMS

reactive-ion etching, PMMA, 2-D materials, residue, MoS_2

16. SECURITY CLASSIFICATION OF:			17. LIMITATION OF ABSTRACT	18. NUMBER OF PAGES	19a. NAME OF RESPONSIBLE PERSON
a. REPORT	b. ABSTRACT	c. THIS PAGE			Alexander L Mazzoni
Unclassified	Unclassified	Unclassified	UU	26	19b. TELEPHONE NUMBER (Include area code) 301-394-0494

Standard Form 298 (Rev. 8/98)
Prescribed by ANSI Std. Z39.18

Contents

List of Figures iv

List of Tables v

Acknowledgments vi

1. Introduction 1

2. Methods/Procedures 2

3. Results 3

3.1 PMMA Age and Composition 4

3.2 RIE Treatment 5

3.3 MoS_2 Etch Capability 7

3.4 Post-Etch Treatments 7

3.5 Secondary Oxygen RIE 9

3.6 Mechanism Discussion 11

4. Conclusion 12

5. References 14

List of Symbols, Abbreviations, and Acronyms 16

Distribution List 17

List of Figures

Fig. 1 CAD drawings of the PMMA mask used during the RIE etch step. The hashed area represents where the PMMA would be removed during resist development, whereas the middle areas would remain for the etching process. 2

Fig. 2 a) AFM height profile of the PMMA flap and b) the RMS roughness for the fully etched region (0.17 nm) and the flap (0.52 nm). After zooming in on the PMMA residue, pebbling can be seen in b) the height and phase AFM images. c) Diagram illustrating the incoming reactive ions interacting with the top layer of the PMMA and graphitizing it. d) Optical image of a device with PMMA residue..... 4

Fig. 3 AFM images of the PMMA residue after $CF_4 + O_2$ RIE using different PMMA types and ages. The zoomed-in areas in a, b, and c show the PMMA residue agglomerations in the corners of the features. The AFM of PMMA 495 A8 in b shows bending and folding in the smaller rectangular mesa region. The SiO_2 control is shown in d. 5

Fig. 4 Optical imaging after RIE and PMMA removal for $CF_4 + O_2$, $Cl_2 + O_2$, and O_2 RIE recipes. The left column shows zoomed-in features of the profile from the CAD drawing in Fig. 1. The outlined areas show the remaining residue after the RIE step. The right column shows a broader view for the $CF_4 + O_2$ and $Cl_2 + O_2$ recipes to emphasize the severity of the resist residue..... 6

Fig. 5 Etching of MoS_2 using various recipes. Recipe shown at the top. Optical images show the same area before and after RIE etching. Different MoS_2 thicknesses were etched and analyzed. 7

Fig. 6 AFM analysis of different post-etch cleaning recipes and their effect on the PMMA residue. The cleaning procedure is written above each set of AFM images, and the RIE recipe is identified on the image in white text. New PMMA 950 A4 was used for all samples. The samples were cleaned in a) room temperature acetone and imaged with AFM, then the same sample was cleaned in b) hot acetone and imaged again. Then the sample was cleaned in c) hot 1165 and imaged with AFM. With the $Cl_2 + O_2$ sample, the PMMA folded over on top of itself. 9

Fig. 7 Effects of a secondary 5-s, 15-sccm, 250-W O_2 RIE cleaning step on the a) $CF_4 + O_2$ recipe and b) $Cl_2 + O_2$ recipe. c) σ_{RMS} for various treatments. 10

Fig. 8 Schematic of the proposed PMMA residue formation process. Development after EBL exposure will remove an area of PMMA on the chip. Then, as the sample is bombarded by reactive ions, a graphitized PMMA layer is formed. The acetone wash then penetrates through the PMMA and removes the underlying PMMA; however, it is unable to remove the graphitized residue that remains attached to the surface. The residues will remain on the top of the sample and will fall onto the surface depending on how it is removed from the solvent bath. After the residue dries on the substrate it is difficult to remove. 12

List of Tables

Table 1 Comparison of different RIE gas chemistries 11

Acknowledgments

This research was supported in part by an appointment to the Student Research Participation Program at the US Army Research Laboratory (ARL) administered by the Oak Ridge Institute for Science and Education through an interagency agreement between the US Department of Energy and ARL.

Alin Cristian Chipara and Alexander L Mazzoni contributed equally as co-first authors for this report.

1. Introduction

Our work at the US Army Research Laboratory (ARL) explores the use of 2-D materials in electronic devices. The fabrication of these devices requires several steps including growth, transfer, lithography, dry etching, and metal deposition. Throughout each step the 2-D material is exposed to a variety of chemicals and polymers. Chemical residues and impurities can act as scattering centers, and impurity scattering is often the dominant mechanism that limits mobility in 2-D materials.[1,2] Therefore, to optimize the electrical properties of the devices, such as doping or mobility, it is important to continuously improve our fabrication processes.

Our current transistor fabrication process relies on poly(methyl methacrylate) (PMMA) for the material transfer off of the growth substrate and for patterning of regions that undergo dry etching and metal lift-off. Previously it has been shown with graphene that the use of PMMA affects the properties of the 2-D layer. For example, the PMMA concentration of the film used to transfer graphene was demonstrated to be important, with higher (lower) concentrations of PMMA leading to higher (lower) p-doping, lower (higher) mobility, and more (less) surface roughness.[3] Pirkle et al. showed that due to incomplete PMMA removal there were changes in the I_{2D} to I_G peak intensity ratio in graphene that led to lowered carrier mobilities and p-type doping of devices.[4] To remove PMMA residue, annealing in a vacuum or forming gas environment is commonly used. However, PMMA removal requires going to temperatures in excess of 300 °C, which has been demonstrated to p-dope graphene[5] except in ultra-high-vacuum conditions.[4] Unfortunately, there is usually still some residue after annealing,[6] and for applications with flexible substrates this heat treatment is often not allowed.

Since polymer interaction with 2-D layers often leads to residues that are difficult to remove, a variety of other methods have been explored to create cleaner devices. For example, researchers have suspended the 2-D channel and performed current annealing,[7] investigated hexagonal boron nitride as an alternative substrate,[8] and developed cleaner pick-up and stack techniques for exfoliated flakes of van der Waals materials.[9] Unfortunately, these techniques are not feasible or developed sufficiently for large-area, batch-processed devices. Current fabrication processing techniques for large-area 2-D materials still often rely on polymers such as PMMA for lithography steps of device fabrication or to perform material transfer from the growth substrate.

Our process for fabricating transistors out of molybdenum disulfide (MoS_2) grown in-house via chemical vapor deposition (CVD) includes the dry-etching of MoS_2 through a PMMA pattern. Previously we have relied on a carbon tetraflouride (CF_4) + oxygen (O_2) reactive-ion etch (RIE) recipe (15 sccm CF_4, 5 sccm O_2, and 200 W) to etch MoS_2. However, we have observed that this process can leave a significant amount of PMMA residue on the substrate surface if the PMMA removal process is not aggressive enough. Additionally, this CF_4 + O_2 process etches silicon dioxide (SiO_2), which is typically used as both the substrate and back-gate dielectric of our 2-D field effect transistors. The PMMA residue tends to form a flap at the edge of the etched region instead of PMMA particulate matter that is commonly reported in the 2-D literature. While this may not come into contact with the channel region, it can still have drawbacks on the overall device reliability. The goal of this report is to investigate the origin of the PMMA residue and develop a new RIE recipe that eliminates or minimizes the polymer residue and etching of the SiO_2 substrate.

2. Methods/Procedures

To investigate the residue issue we fabricated several PMMA mesa structures and performed test etches while varying the PMMA age, composition, RIE gases, as well as the PMMA removal process.

Computer aided design (CAD) drawings of the test patterns used are shown in Fig. 1. Each structure consisted of a large square (200 × 200 μm) that would be etched and an inner protected region that was either a small square (10 × 10 μm) or rectangle (1 × 5 μm). A square and a rectangle were chosen to compare the 2 geometries and determine if their dimensions impacted the etching process.

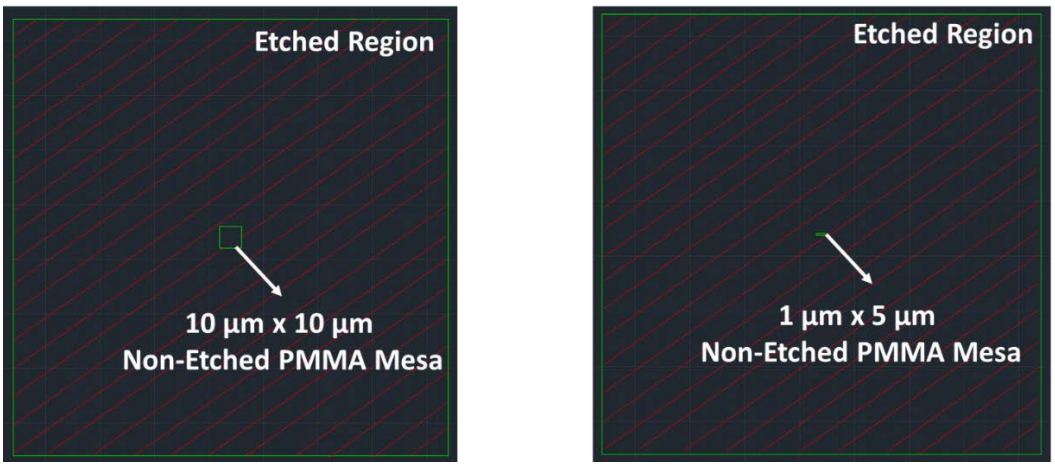

Fig. 1 CAD drawings of the PMMA mask used during the RIE etch step. The hashed area represents where the PMMA would be removed during resist development, whereas the middle areas would remain for the etching process.

For all patterning, the PMMA was spun at 2000 rpm and baked on a hot plate at 180 °C for 2 min to cure the resist. All patterning of PMMA was done via electron beam lithography (EBL; Vistec EBPG5000+) with an exposure dose of 850 $\mu C/cm^2$ and development in 25 mL of isopropyl alcohol (IPA): 10 mL methyl isobutyl ketone for 75 s.

The standard RIE (performed using an Ulvac NE550e) step consisted of a 200-W, 45-s, 15-sccm CF_4, and 5-sccm O_2 etch. After etching, PMMA was removed by an overnight soak in acetone followed by an IPA rinse and drying with nitrogen.

The topography of our samples was investigated via atomic force microscopy (AFM) using a Veeco Nanoman V in tapping mode.

3. Results

Our devices exhibited flap-like structures around the dry-etched area, which we attributed to the PMMA etch mask hardening during our standard RIE process (Fig. 2). This residue is very similar to that observed by Koval et al.[10] and Oehrlein et al. in terms of topography and size.[11] Other papers have shown that the use of RIE can cause the PMMA to exhibit pebbling and become difficult to remove.[11] AFM revealed the flaps to be about 5 nm thick with a pebble-like structure. Oehrlein et al. suggested that the reason for this is the graphitization of the top layer of the PMMA due to the energy of the reactive ions interacting with the surface layer (Fig. 2).[11]

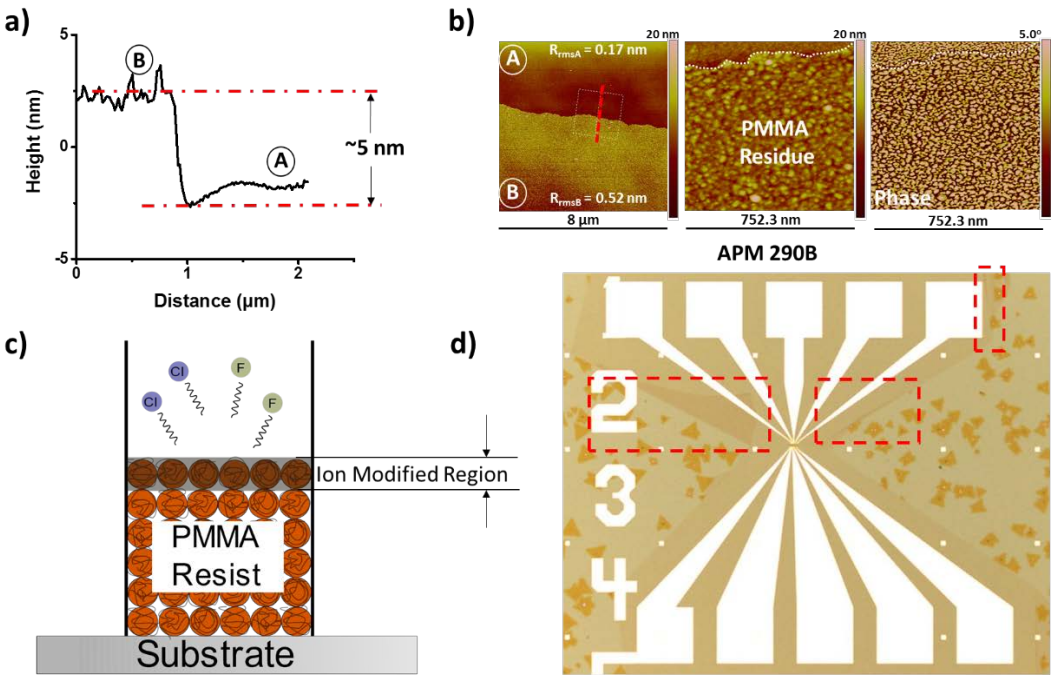

Fig. 2 a) AFM height profile of the PMMA flap and b) the RMS roughness for the fully etched region (0.17 nm) and the flap (0.52 nm). After zooming in on the PMMA residue, pebbling can be seen in b) the height and phase AFM images. c) Diagram illustrating the incoming reactive ions interacting with the top layer of the PMMA and graphitizing it. d) Optical image of a device with PMMA residue.

3.1 PMMA Age and Composition

In our initial experiments, we investigated different types of PMMA (950 A4 and 495 A8) and different ages of PMMA 950 A4 (2006 vs. 2017) to determine if PMMA type or age affects the etching process. The numbers 950 and 495 refer to the molecular weight of the PMMA (950,000 and 495,000, respectively). A4 and A8 refer to the concentration of the PMMA in the solvent anisole (4% and 8% in anisole, respectively). Higher molecular weight and PMMA concentrations create a more viscous fluid that, when spin-coated, results in a thicker film.

To explore the impact of the PMMA age and composition, we used AFM to image the mesas after RIE of the regions. The age of the PMMA did not appear to have a noticeable effect on the resulting mesa (Figs. 3a and c), but there was a significant difference in the final mesa topography when using 950 A4 versus 495 A8 (Figs. 3a and b). Both PMMA A4 and A8 were spun at 2000 rpm (300 nm for A4 and 650 nm for A8), but PMMA A8 led to warping of the patterned structures due to a significant increase in viscosity compared with A4. However, all of the PMMA compositions exhibited PMMA agglomerations at the corners of the mesa regions, which could contribute to contamination and strain in devices among other negative

effects. Since the A8-based samples were warped, we chose to use the new PMMA 950 A4 as our standard for the all later experiments such as varying the RIE recipe or removal processes.

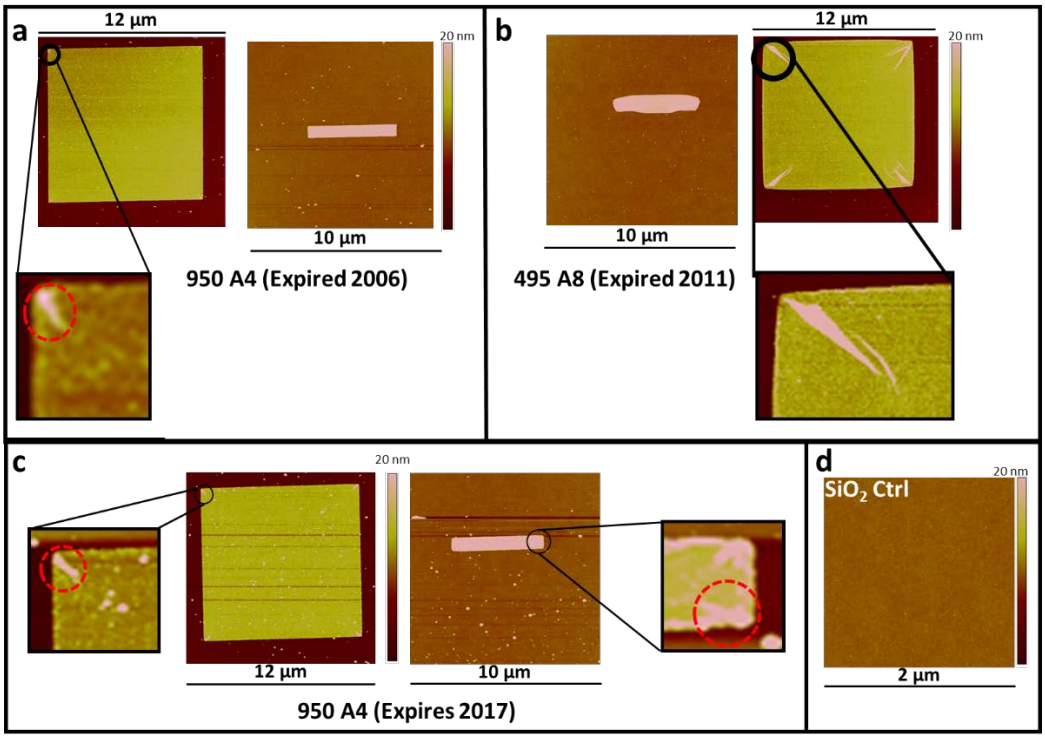

Fig. 3 AFM images of the PMMA residue after $CF_4 + O_2$ RIE using different PMMA types and ages. The zoomed-in areas in a, b, and c show the PMMA residue agglomerations in the corners of the features. The AFM of PMMA 495 A8 in b shows bending and folding in the smaller rectangular mesa region. The SiO_2 control is shown in d.

3.2 RIE Treatment

After determining the effects of the PMMA type and age, we started optimizing the RIE parameters in an attempt to resolve the PMMA residue issue. We tested several RIE gas chemistries including our $CF_4 + O_2$ standard (15 sccm CF_4 + 5 sccm O_2 for 45 s at 200 W), chlorine (Cl_2) + O_2 (15 sccm Cl_2 + 5 sccm O_2 for 45 s at 200 W), and O_2 (15 sccm, 20 s at 200 W + 20 s at 250 W). The O_2 recipe failed midway through the process, which is why there are two 20-s steps, one at 200 W and another at 250 W. Since we saw the residue flaps using $CF_4 + O_2$, it was designated as our control sample. Cl_2 was chosen as one of the alternative chemistries since it does not etch the SiO^2 layer,[12] which is important for device reliability since it minimizes leakage effects. O_2 was picked due to its ability to remove graphitized layers.[13] PMMA 950 A4 was spun onto several SiO_2/Si chips, and the pattern from Fig. 1 was written using EBL. After developing the resist, each chip was exposed to a different RIE gas chemistry. After an overnight soak in acetone, followed by

an IPA rinse and drying the sample with nitrogen, optical microscopy and AFM were performed on the chips. The optical images in Fig. 4 show that both the CF_4 + O_2 and Cl_2 + O_2 etch recipes produce flaps and exhibit large amounts of PMMA residue, while O_2 leaves little to no residue. The CF_4 + O_2 etch exhibits less residue than the Cl_2 + O_2 etch, but it did remove some of the oxide layer unlike the Cl_2 + O_2 etch.

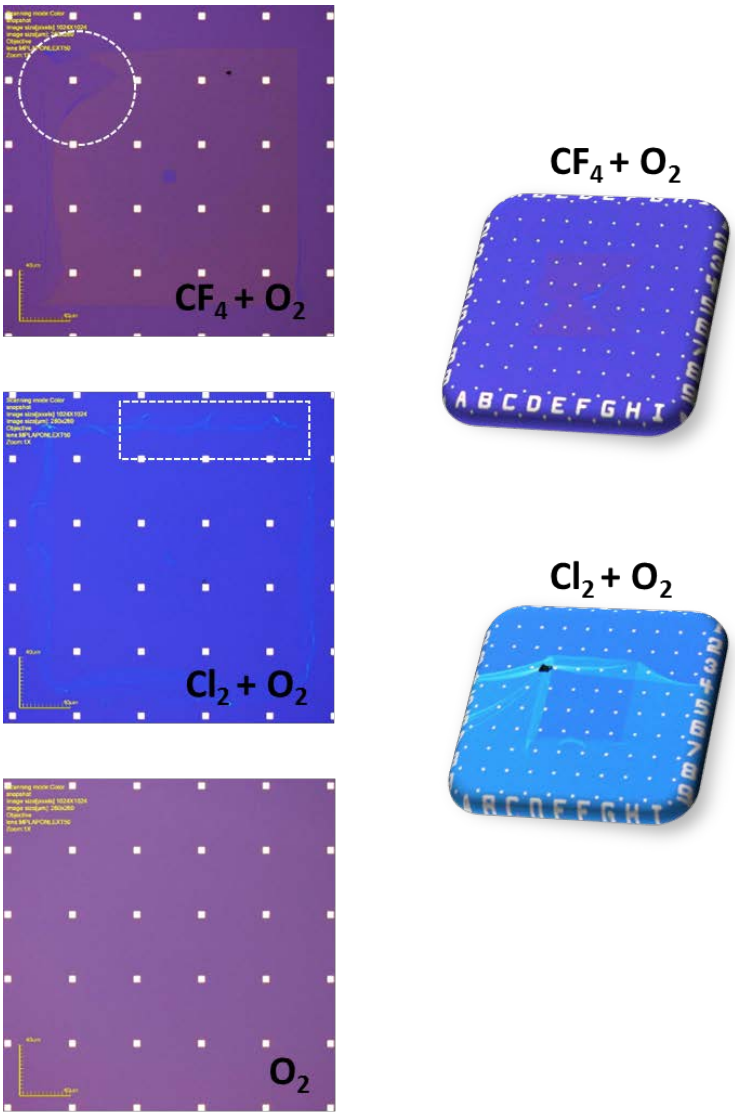

Fig. 4 Optical imaging after RIE and PMMA removal for CF_4 + O_2, Cl_2 + O_2, and O_2 RIE recipes. The left column shows zoomed-in features of the profile from the CAD drawing in Fig. 1. The outlined areas show the remaining residue after the RIE step. The right column shows a broader view for the CF_4 + O_2 and Cl_2 + O_2 recipes to emphasize the severity of the resist residue.

3.3 MoS_2 Etch Capability

While it is important for the RIE recipe to limit hardening of the PMMA and etching of SiO_2, it is also paramount that it can successfully etch MoS_2. Therefore, we investigated the MoS_2 etch capability using the different RIE recipes (Cl_2 + O_2 and O_2 chemistries) on material grown by CVD. CF_4 was already known to be capable of etching MoS_2 and served as a benchmark. Initial tests with Cl_2 + O_2 at 200 W (left side, Fig. 5) showed efficient etching of monolayer MoS_2; however, thicker areas such as the string-like structures remained. Raising the power of the Cl_2 + O_2 recipe to 250 W successfully removed the thicker areas of MoS_2 (Fig. 5, left side). When etching with O_2 we found it difficult to etch thicker layers of MoS_2 and could only efficiently etch MoS_2 monolayers (Fig. 5, right side).

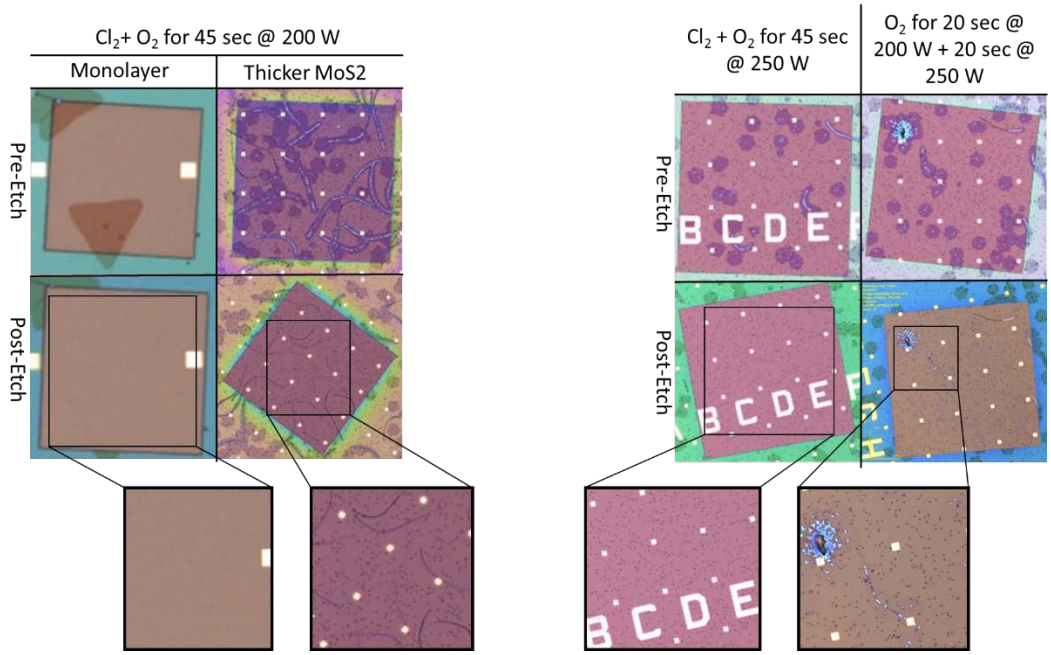

Fig. 5 Etching of MoS_2 using various recipes. Recipe shown at the top. Optical images show the same area before and after RIE etching. Different MoS_2 thicknesses were etched and analyzed.

3.4 Post-Etch Treatments

In an attempt to find a solution for the flaps and mesa region residue, we looked at 2 different approaches: chemical solvents and additional dry etching steps. The first approach relied on post-etch treatments utilizing different solvents and heating of the solvents. Besides room temperature acetone, we also tried heating the acetone to 60 °C, since many researchers have shown improved removal of the resist by heating it.[14,15] We also investigated a heated solution of Microposit Remover 1165

(1-methyl-2-pyrrolidinone, or 1165 for short) as an alternative to acetone. We started with a baseline cleaning by soaking the processed chips (different etch chemistries of $Cl_2 + O_2$, $CF_4 + O_2$, and O_2) in acetone overnight. We then performed AFM on the cleaned samples, after which we placed them in a hot acetone bath (60 °C) for 1 h. After the soak was complete we carried out AFM again to observe if there were any changes in surface roughness compared with the overnight acetone soak. The final clean involved soaking the samples in 1165 at 60 °C for 1 h. Then we performed AFM to investigate the presence of any changes from the 1165 soak. Hot acetone was found to remove many of the residual surface particles that the overnight soak left behind (Figs. 6a and b). The AFM data, however, showed almost no difference between the hot acetone and 1165 treatments (Fig. 6c). None of the post-etch treatments showed the ability to fully remove the flaps chemically, suggesting that the flaps exhibit a significantly different chemical structure than PMMA. On the other hand, these flaps can be physically removed through excessive heating of acetone (>60 °C), squirting the sample with solvent, or sonication. However, by using these physical procedures, there is a larger risk that the quality and structural integrity of the 2-D layer may be negatively affected.

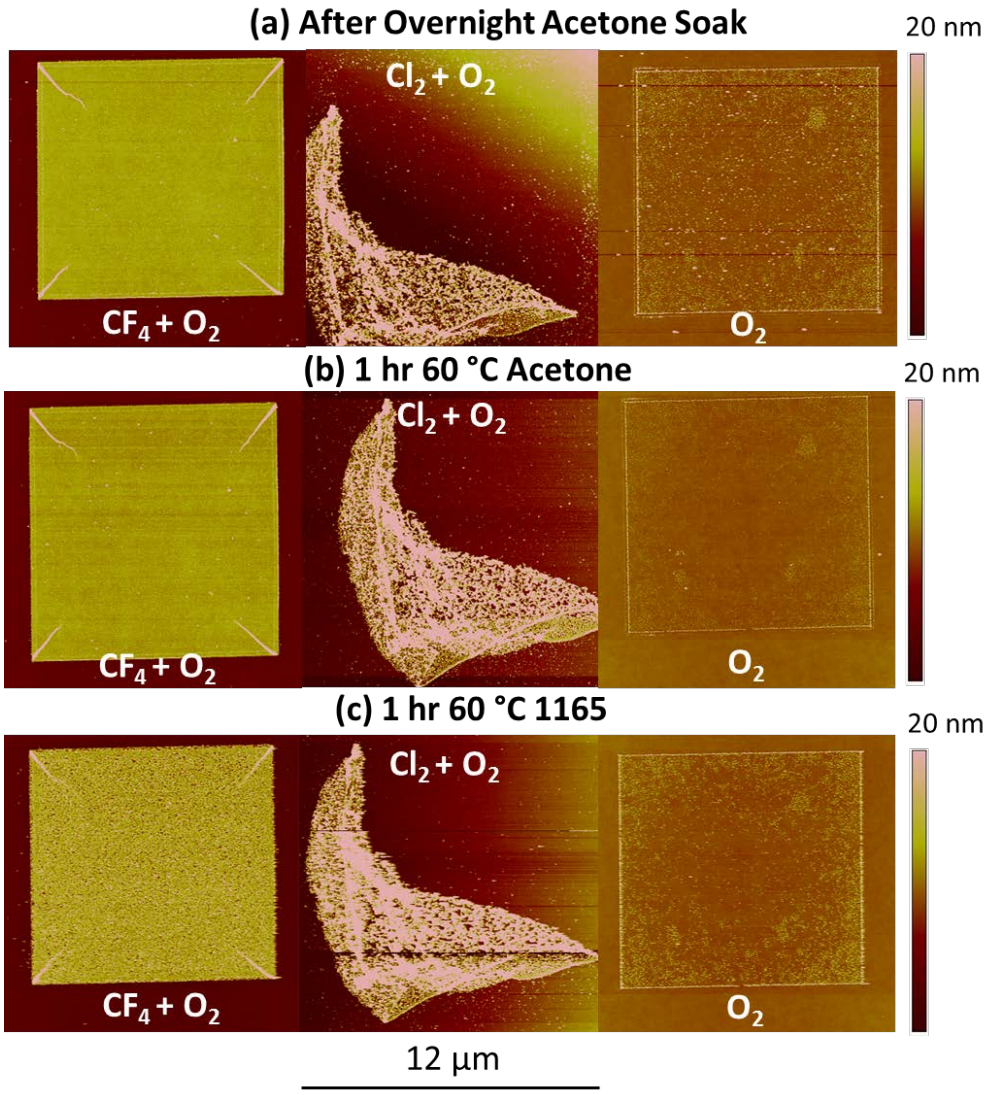

Fig. 6 AFM analysis of different post-etch cleaning recipes and their effect on the PMMA residue. The cleaning procedure is written above each set of AFM images, and the RIE recipe is identified on the image in white text. New PMMA 950 A4 was used for all samples. The samples were cleaned in a) room temperature acetone and imaged with AFM, then the same sample was cleaned in b) hot acetone and imaged again. Then the sample was cleaned in c) hot 1165 and imaged with AFM. With the $Cl_2 + O_2$ sample, the PMMA folded over on top of itself.

3.5 Secondary Oxygen RIE

The second approach to reduce/remove the PMMA residue relied on adding a secondary RIE step that used a pure O_2 recipe (15 sccm, 5 s, at 250 W) to remove the hardened PMMA. As previously mentioned, O_2 should be able to remove any graphitized layer that would form on the surface.[14] The O_2 etch recipe was applied after the initial RIE, and the secondary O_2 step was found to remove the agglomerations in the corners as well as the previously seen flaps for both $CF_4 + O_2$ and $Cl_2 + O_2$ etched samples (Figs. 7a and b).

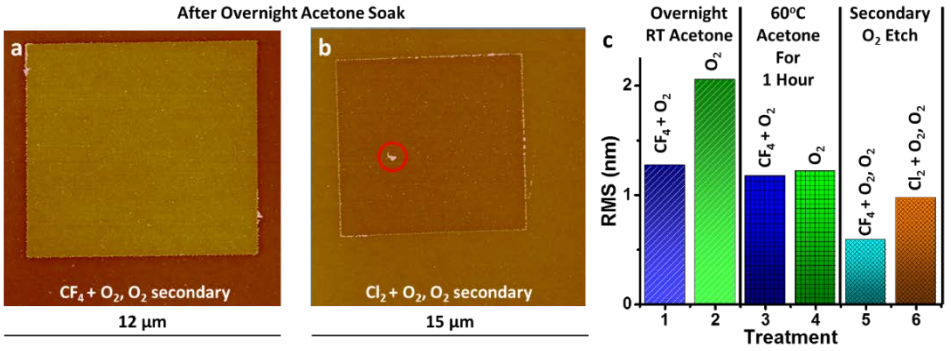

Fig. 7 Effects of a secondary 5-s, 15-sccm, 250-W O_2 RIE cleaning step on the a) $CF_4 + O_2$ recipe and b) $Cl_2 + O_2$ recipe. c) σ_{RMS} for various treatments.

We believe that when the O_2 was combined with CF_4 or Cl_2, residue was observed because the rate of removal of hardened PMMA was lower than the rate at which the CF_4 or Cl_2 hardened the top PMMA layer. To further analyze the data, we looked at the root-mean-square (RMS) surface roughness (σ_{RMS}) values for the mesa region after undergoing the aforementioned treatments. The AFM data was flattened using the built-in software Nanoscope 7.30. Then the data was exported, and the RMS data for the mesa region was analyzed by drawing a mask over the mesa area with the image software Gwyddion. This allowed us to fully analyze the mesa region and minimize deviations that arise from moving between the etched and nonetched region of the sample. The $CF_4 + O_2$ etch with the secondary O_2 step showed the best results with an average surface roughness of approximately 0.59 nm (Fig. 7c). However, the $Cl_2 + O_2$ recipe with the secondary O_2 step also showed very low surface roughness (0.97 nm), which reaches parity with the aforementioned recipe if we neglect the impact of the large residue chunk (Fig. 7b). Compared with previous AFM data taken in this experiment, the largest variability in surface roughness was seen in the O_2 recipe with an overnight acetone soak (2.05 nm) (Fig. 7c). It is also clear that hot acetone is much better at removing surface debris than regular acetone as shown by the surface roughness reduction in both the $CF_4 + O_2$ (7.6% decrease in σ_{RMS}) samples and the O_2 (40.7% decrease in σ_{RMS}) etched samples. The room temperature acetone baseline clean exhibits an average roughness of 1.66 nm. By using hot acetone the roughness drops to 1.2 nm with a very small differences between the different etch samples (~3%). Of the etching processes, the best method to minimize surface roughness is using a secondary O_2 etch step. Performing the secondary O_2 etch step reduces the surface roughness further to about 0.78 nm. This implies that the samples undergo a stepwise removal of various particulates (i.e., hot acetone removes more particulates than room temperature acetone but much less than the secondary O_2 etch step). RMS data for the Cl_2 sample are not compared because the residue flaps are large and folded on top of each other, distorting the results.

Table 1 outlines the pros and cons of each gas recipe for etching MoS_2 on SiO_2. As can be seen, both the $CF_4 + O_2$ and the $Cl_2 + O_2$ recipes are suitable for etching thicker MoS_2; however, they also harden the PMMA mask, which can lead to the observed residue. Additionally, $CF_4 + O_2$ has been shown to etch SiO_2, while $Cl_2 + O_2$ does not etch the oxide layer. The pure O_2 recipe cannot etch thicker MoS_2 and does not etch the oxide layer. To achieve all the desired results for our mesa etch, the $Cl_2 + O_2$ etch with a secondary O_2 step was chosen (Table 1, last column).

Table 1 Comparison of different RIE gas chemistries

Effect	$CF_4 + O_2$	$Cl_2 + O_2$	O_2	$CF_4 + O_2$, O_2	$Cl_2 + O_2$, O_2
Etches monolayer MoS_2	✓	✓	✓	✓	✓
Etches multilayer MoS_2	✓	✓	×	✓	✓
Does not etch SiO_2	×	✓	✓	×	✓
No hardened PMMA residue	×	×	✓	✓	✓

3.6 Mechanism Discussion

The schematic in Fig. 8 shows the expected mechanism for the formation of the PMMA flaps and residue. Initially, we start with a PMMA-coated substrate that is patterned using EBL to match our CAD design. Next, the RIE process is performed, during which the sample is bombarded by reactive ions. This causes the top layer of PMMA to harden and graphitize. The specific mechanism for the hardening is as yet unknown; however, there are several theories mentioned in papers such as Koval et al.[10] and Oehrlein et al.[11] Most researchers agree that this is not a localized heating issue and is a reaction to the high-energy reactive particles that are impacting the surface. This tends to lead to polymer scission, which exposes reactive sites that can cause hardening or graphitization. After the RIE process, the samples were imaged and showed no residue on the exposed SiO_2 area. Residue is seen only after PMMA removal in solvent. Because of the lack of residue after etching, we believe the meeting points between the substrate, polymer, and etch process act as an anchoring location for the residue itself. As the material is left in an acetone bath, the PMMA that was not graphitized is removed, leaving behind a graphitized PMMA layer that is anchored to the substrate surface. The hardened PMMA layer cannot be removed with room temperature acetone baths and requires sonication/heated acetone (>60 °C) or direct squirting to remove. When the sample is removed from the solvent baths, the flaps adhere to the substrate as the solvents evaporate.

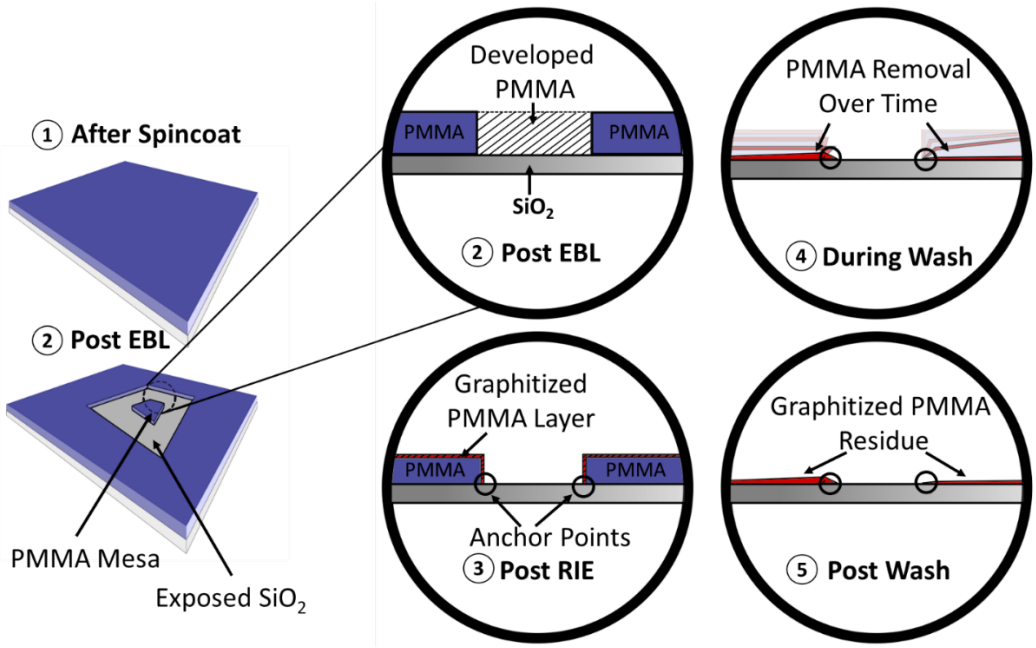

Fig. 8 Schematic of the proposed PMMA residue formation process. Development after EBL exposure will remove an area of PMMA on the chip. Then, as the sample is bombarded by reactive ions, a graphitized PMMA layer is formed. The acetone wash then penetrates through the PMMA and removes the underlying PMMA; however, it is unable to remove the graphitized residue that remains attached to the surface. The residues will remain on the top of the sample and will fall onto the surface depending on how it is removed from the solvent bath. After the residue dries on the substrate it is difficult to remove.

4. Conclusion

We have shown that RIE can lead to PMMA residue in our device fabrication process, since the RIE will graphitize the top layer of PMMA. In our case, the PMMA residue takes the form of a flap rather than as general particulates. If an additional O_2 RIE step is added, the graphitized PMMA can be effectively removed. Other observations from our study include the following:

- The observed residue did not depend on the age (2006 vs. 2017) of the PMMA used; however, it was worse for thicker PMMA films.
- Both CF_4 and Cl_2 RIE processes led to the formation of the residue flaps; however, O_2 processes did not.
- Heated acetone and 1165 were not able to chemically remove the residue, indicating that the flaps left on the wafer surface were significantly modified from the original PMMA structure.

- 1 h of heated acetone (60 °C) demonstrated an improvement in removal of particulate residue compared with an overnight soak in room temperature acetone.
- Both CF_4 and Cl_2 RIE processes could etch thicker regions of MoS_2; however, O_2 could only etch monolayer regions.
- CF_4 RIE processes etch SiO_2, which is commonly used as a substrate and back-gate dielectric, whereas Cl_2 and O_2 do not.
- By adding a secondary 5- to 10-s O_2 step to the CF_4 or Cl_2 RIE processes, the residue flaps are completely removed.

Going forward, we are switching from the CF_4 RIE recipe to a Cl_2 process with a secondary O_2 step. This process improvement ensures no hardened PMMA residue will be present and that the SiO_2 substrate and back-gate dielectric will be better protected.

5. References

1. Chen J, Jang C, Xiao S, Ishigami M, Fuhrer MS. Intrinsic and extrinsic performance limits of graphene devices on SiO_2. Nat Nanotechnol. 2008;3: 8–11.

2. Ma N, Jena D. Charge scattering and mobility in atomically thin semiconductors. Phys Rev X. 2014;4:1–9.

3. Suk JW, Lee WH, Lee J, Chou H, Piner RD, Hao Y, Akinwande D, Ruoff RS. Enhancement of the electrical properties of graphene grown by chemical vapor deposition via controlling the effects of polymer residue. Nano Lett. 2013;13:1462–1467.

4. Pirkle A, Chan J, Venugopal A, Hinojos D, Magnuson CW, McDonnell S, Colombo L, Vogel EM, Ruoff RS, Wallace RM. The effect of chemical residues on the physical and electrical properties of chemical vapor deposited graphene transferred to SiO_2. Appl Phys Lett. 2011;99:122108.

5. Cheng Z, Zhou Q, Wang C, Li Q, Wang C, Fang Y. Toward intrinsic graphene surfaces: a systematic study on thermal annealing and wet-chemical treatment of SiO_2-supported graphene devices. Nano Lett. 2011;11:767–771.

6. Lin Y-C, Lu C-C, Yeh C-H, Jin C, Suenaga K, Chiu P-W. Graphene annealing: How clean can it be? Nano Lett. 2012;12: 414–419.

7. Bolotin KI, Sikes KJ, Jiang Z, Klima M, Fudenberg G, Hone J, Kim P, Stormer HL. Ultrahigh electron mobility in suspended graphene. Solid State Commun. 2008;146:351–355.

8. Burson KM, Cullen WG, Adam S, Dean CR, WatanabeK, Taniguchi T, Kim P, Fuhrer MS. Direct imaging of charged impurity density in common graphene substrates. Nano Lett. 2013;13:3576–3580.

9. Pizzocchero F, Gammelgaard L, Jessen BS, Caridad JM, Wang L, Hone J, Bøggild P, Booth TJ. The hot pick-up technique for batch assembly of van der Waals heterostructures. Nat Commun. Published online; 2016 June 16. doi:10.1038/ncomms11894.

10. Koval Y. Mechanism of etching and surface relief development of PMMA under low-energy ion bombardment mechanism of etching and surface relief development of PMMA under low-energy ion bombardment. J Vac Sci Technol B Microelectron Nanom Struct Process Meas Phenom. 2004;843. doi:10.1116/1.1689306.

11. Oehrlein GS, Phaneuf RJ, Graves DB. Plasma-polymer interactions: a review of progress in understanding polymer resist mask durability during plasma etching for nanoscale fabrication. J Vac Sci Technol B. 2011;29:1–35.

12. Vanderlinde WE, Von Benken CJ. Rapid integrated circuit delayering without grass. Proceedings of the International Society for Optics and Phontonics (SPIE). 1996;2874:260–271.

13. Lu X, Huang H, Nemchuk N, Ruoff RS. Patterning of highly oriented pyrolytic graphite by oxygen plasma etching. Appl Phys Lett. 1999;75:193–195.

14. Guimaraes MHD, Gao H, Han Y, Kang K, Xie S, Kim C-J, Muller DA, Ralph DC, Park J. Supplementary information for atomically thin ohmic edge contacts between two-dimensional materials. ACS Nano. 2016;10:6392–6399.

15. Resta GV, et al. Polarity control in WSe_2 double-gate transistors. Sci. Rep. 2016;6:1–6.

List of Symbols, Abbreviations, and Acronyms

1165	Microposit Remover 1165 (1-methyl-2-pyrrolidinone)
σ_{RMS}	root-mean-square surface roughness
2-D	2-dimensional
AFM	atomic force microscopy
ARL	US Army Research Laboratory
CAD	computer-aided design
CF_4	carbon tetrafluoride
Cl_2	chlorine
CVD	chemical vapor deposition
EBL	electron beam lithography
IPA	isopropyl alcohol
MoS_2	molybdenum disulfide
O_2	oxygen
PMMA	poly(methyl methacrylate)
RIE	reactive-ion etching
RMS	root mean square
SiO_2	silicon dioxide

1 (PDF) DEFENSE TECHNICAL INFORMATION CTR DTIC OCA

2 (PDF) DIR ARL
RDRL DCM
IMAL HRA RECORDS MGMT
RDRL DCL
TECH LIB

1 (PDF) GOVT PRINTG OFC
A MALHOTRA

18 (PDF) DIR ARL
RDRL DE
T O'REGAN
RDRL SER L
A MAZZONI
M CHIN
R BURKE
M DUBEY
W NOTHWANG
B NICHOLS
E ZAKAR
S NAJMAEI
C KNICK
RDRL SEE
P SUNAL
M ROY
N MARK
RDRL SER E
J WEIL
T IVANOV
G BIRDWELL
P SHAH
F CROWNE

INTENTIONALLY LEFT BLANK.